Electropore Formation in Mechanically Constrained Phospholipid Bilayers

M. Laura Fernández[1,2,3] · Marcelo Raúl Risk[3,4] · P. Thomas Vernier[5]

Abstract
Molecular dynamics simulations of lipid bilayers in aqueous systems reveal how an applied electric field stabilizes the reorganization of the water–membrane interface into water-filled, membrane-spanning, conductive pores with a symmetric, toroidal geometry. The pore formation process and the resulting symmetric structures are consistent with other mathematical approaches such as continuum models formulated to describe the electroporation process. Some experimental data suggest, however, that the shape of lipid electropores in living cell membranes may be asymmetric. We describe here the axially asym-metric pores that form when mechanical constraints are applied to selected phospholipid atoms. Electropore formation pro-ceeds even with severe constraints in place, but pore shape and pore formation time are affected. Since lateral and transverse movement of phospholipids may be restricted in cell membranes by covalent attachments to or non-covalent associations with other components of the membrane or to membrane-proximate intracellular or extracellular biomolecular assemblies, these lipid-constrained molecular models point the way to more realistic representations of cell membranes in electric fields.

Keywords Phospholipid bilayer · Electroporation · Position constraints · Molecular dynamics

Introduction

The normal selective permeability of the cell membrane can be affected by an external pulsed electric field, a phenomenon known as electroporation or electropermeabilization (Tsong 1991). Electroporation applications, which include biomedical procedures (Breton and Mir 2012; Yarmush et al. 2014) and biotechnological and industrial processes (Kotnik et al. 2015), depend on the transport across the membrane of normally impermeant molecules (pharmacological agents, nucleic acids, inorganic ions). Despite the importance and widespread utilization of electroporation technology, the molecular mechanisms for transport are understood today only at a rudimentary level. The dominant electroporation model posits the formation of transient defects (aqueous pores) under the influence of supraphysiological transmembrane voltages induced by an externally applied electric field (Sugar and Neumann 1984; DeBruin and Krassowka 1999, Weaver 2000), which can vary in duration, intensity, and frequency (Silve et al. 2014).

The nanoscale phenomena occurring during pore formation in a lipid bilayer exposed to an external electric field are difficult to evaluate and quantify experimentally, but molecular dynamics (MD) simulations have revealed that pore formation is initiated by intrusions of interfacial water into the bilayer interior. These water fingers are stabilized by the porating electric field, which facilitates their extension across the membrane to form water bridges, the "hydrophobic pores" of standard electroporation models. Phospholipid head groups follow the water within nanoseconds, surrounding the aqueous columns spanning the membrane to form "hydrophilic pores." If the external electric field is removed, the pore creation process is reversed, and the membrane

✉ P. Thomas Vernier
pvernier@odu.edu

1 Universidad de Buenos Aires, Facultad de Ciencias Exactas y Naturales, Departamento de Física, Buenos Aires, Argentina

2 CONICET - Universidad de Buenos Aires, Instituto de Física del Plasma (INFIP), Buenos Aires, Argentina

3 Consejo Nacional de Investigaciones Científicas y Técnicas (CONICET), Buenos Aires, Argentina

4 Instituto Tecnológico de Buenos Aires (ITBA), Buenos Aires, Argentina

5 Frank Reidy Research Center for Bioelectrics, Old Dominion University, Norfolk, VA, USA

barrier is restored (Tieleman 2004; Tarek 2005; Levine and Vernier 2010).

Although lipid electropore structure has never been observed directly, models and experiments suggest some features of electropore geometry. Both atomistic and coarse-grained molecular dynamics models of lipid pores formed by a variety of methods—dimethyl sulfoxide destabilization of the lipid bilayer, ion transmembrane charge imbalance, pore-forming peptides, mechanical displacement of lipid head groups into the bilayer interior, electroporation, application of lateral tension, or local density constraints—assume a similar toroidal shape (Marrink et al. 2009). Continuum models of electropores have evolved from simple cylinders to trapezoidal and toroidal geometries that can be seen as functional representations of the structures that form in molecular models (Weaver and Chizmadzhev 1996, Smith and Weaver 2011, Son et al. 2014). In most molecular and continuum models the pores are geometrically symmetrical both around the pore axis and with respect to the mid-plane of the bilayer.

Living cell membranes are asymmetrical in the composition of the inner and outer leaflets of the lipid bilayer, and there are many differences between the physical environments and the biomolecular landscapes on the exterior and interior faces of the membrane, so we might expect that permeabilizing structures (including pores) in cell membranes are not symmetrical. It has been suggested, for example, that experimental observations of ion current rectification in cells permeabilized by nanosecond electric pulses or in nanofabricated pores could be explained by an asymmetry in pore geometry (Pakhomov et al. 2009; Siwi et al. 2002), and this idea has been incorporated into some pore models (Kotulska et al. 2010; Joshi and Hu 2010).

Local asymmetries in membrane composition can also be involved in transbilayer communication through signaling or structural responses. For example, localized phase domains or clustering in one leaflet can promote the formation of local features in the distal monolayer (Kiessling et al. 2006; Raghupathy et al. 2015). Molecular simulations indicate that liquid-disordered regions of the membrane are electroporated more easily than liquid-ordered regions (Reigada 2014) and that asymmetry in bilayer composition can be associated with leaflet-specific initiation of electropore formation (Gurtovenko and Lyulina 2014). Both lateral and transverse asymmetries in membrane composition and structure imply mechanical asymmetries as well.

In molecular simulations membrane mechanical properties can be modified with atomic resolution using position constraints. Position constraints have been used to introduce artificial pores of different sizes into vesicles, enabling phospholipid translocation (flip-flop) and equilibration of the lipid distribution between the two leaflets (Risselada et al. 2008). The constrained intrusion of a single phosphatidylcholine head group into the bilayer interior causes a water defect and pore formation, from which the free energy of pore formation and of lipid flip-flop (translocation) can be calculated (Sapay et al. 2009). Constraints were imposed to study the partitioning of amino acid analogs and the water defects associated with hydrating the polar and charged residues in a lipid bilayer (MacCallum et al. 2008), and to obtain a cylindrical hydrophobic pore or a toroidal hydrophilic pore as initial configurations for peptide insertion (Mihajlovic and Lazaridies 2010). In other work the mass of head group phosphorus atoms was increased in order to immobilize certain lipids in a bilayer (Raghupathy et al. 2015). Water does not penetrate to the membrane interior when omnidirectional constraints are applied to the carbon atoms of the lipid tails (Sun et al. 2011). Ingólfsson et al. (2014) developed a high complexity bilayer model by coarse-grained simulation to represent a realistic mammalian plasma membrane composed of 63 different lipid species, where in order to prevent the undulations found in large bilayer simulations a weak position restraint was imposed to some lipid to consider the interaction with the cytoskeleton.

We explore symmetry in lipid electropore formation by applying mechanical constraints to the phosphorus atom of lipid head groups on the cathodic side, the anodic side, or both sides of the membrane. We show that restricting lipid movement increases the minimum porating electric field (the minimum electric field intensity needed to open a pore in a lipid bilayer simulation), and that the effect is similar for cathodic- and anodic-side restriction, producing in both cases axially asymmetric, hydrophilic pores, in contrast with the symmetric pores formed when there are no constraints.

The constraints in our simulations are intended to represent in a simple and general way the actual constraints on components of the living cell membrane, through cytoskeletal attachments and other protein–lipid associations, which have been suspected for a long time to play a significant role in electroporation-related phenomena (Rols and Teissié 1992; Berghöfer et al. 2009; Stacey et al. 2011; Chopinet et al. 2014; Kanthou et al. 2006).

Methods

Simulations and Structures

Simulations of bilayer systems containing 128 1-palmitoyl-2-oleoyl-sn-glycero-3-phosphocholine (POPC) molecules were hydrated with water molecules and were carried out using GROMACS 4.5.5 (Hess et al. 2008). POPC topologies from the united-atom force field (Berger et al. 1997) were used. For this work the well-established Berger lipid force field was used. Comparative or more rigorous investigations may necessitate implementation of updated GROMOS

parameters, such as the recently developed united-atom models for dipalmitoylphosphatidylcholine and dimyristoylphosphatidylcholine (Lyubartsev and Rabinovich 2016) or other force fields such as CHARMM36. It must always be understood that the properties of the force fields used for lipid bilayer simulations can affect the results, as has been recently reviewed by Ollila and Pabst (Ollila and Pabst 2016). The simple point charge (SPC) model for water was used (Berendsen et al. 1981). The v-rescale thermostat was used for the temperature ($T = 310$ K) with a relaxation time of 0.1 ps, and the Berendsen pressure coupling (1 atm) with a relaxation time of 1 ps was used in the NPT ensemble (Berendsen et al. 1984). Pressure was coupled semi-isotropically in the *XY* plane and *Z*-direction. The cutoff for short-range electrostatic and Lennard–Jones interactions was 1.0 nm. The PME method (Essman et al. 1995) was used to calculate long-range electrostatics using FFT with a real space cutoff of 1.0 nm, a four-order β-spline interpolation, and a direct-sum tolerance of 10^{-5}. The SETTLE algorithm (Miyamoto and Kollman 1992) was applied to bond lengths in water molecules and the LINCS algorithm to lipid bond lengths (Hess et al. 1997). Periodic boundary conditions in all directions were applied. The time step was 2 fs. The area per lipid was monitored until it fluctuated around a stable value. The last frame of this equilibrated system was used for the initial configuration of a second simulation where an external electric field was applied in the *z*-direction. Position constraints along the *z*-axis (normal to the plane of the bilayer) were imposed on the phosphorus atoms in the POPC bilayers using a force constant of 1000 kJ/mol/nm^2 in the *z*-direction. The polarity of the electric field simulated by GROMACS determines the cathodic and anodic side of the membrane (here the upper and lower leaflet, respectively) (Fig. 1). Four constraint conditions were applied (Fig. 1): no constraint (NC); all phosphorus atoms in both leaflets of the membrane, i.e., anodic and cathodic constraints (ACC); all phosphorus atoms in the cathodic leaflet (CC); all phosphorus atoms in the anodic leaflet (AC).

We developed two systems: a small system containing 128 POPC molecules hydrated with 4480 water molecules, and a large system containing 128 POPC molecules hydrated with 8443 water molecules.

In the small system MD simulations were performed for each constraint condition for 25 ns, applying a transverse electric field from 300 MV/m in steps of 25 MV/m, 5 repetitions for each electric field, in order to find the minimum porating electric field (E_0), i.e., the minimum electric field applied to the bilayer that induces the formation of a pore within a certain simulation time (Ziegler and Vernier 2008). After determining E_0 for each condition, additional simulations were carried out with the electric field applied in steps of 50 MV/m (5 repetitions at each step) for two additional electric field conditions, $E_0 + 50$ MV/m, $E_0 + 100$ MV/m to verify that the increasing electric field increases the number of simulations that opens a pore in 25 ns and to follow the development of the pores in all constraint conditions.

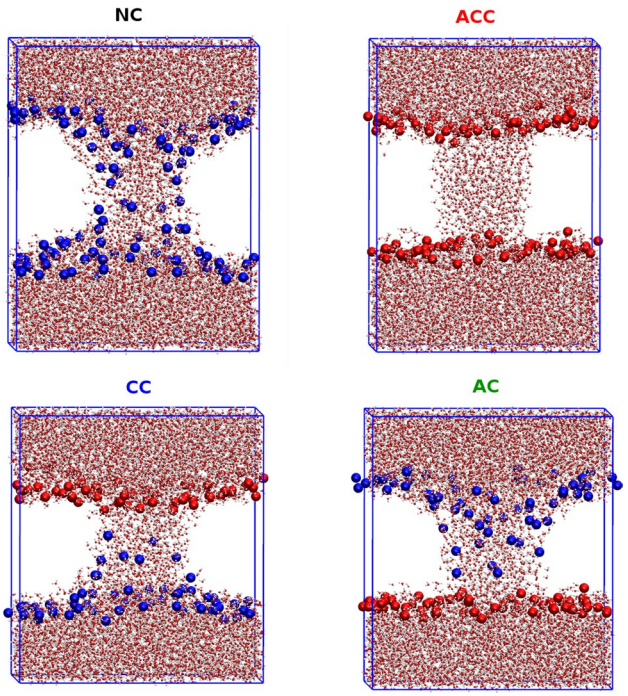

Fig. 1 Representative snapshots of pores obtained with different constraint conditions, where the upper side is the cathode (negative pole), and the lower side is the anode (positive pole). *NC* no constraint, *ACC* anodic and cathodic constraint, *AC* anodic constraint, *CC* cathodic constraint. Blue spheres—unconstrained phosphorus atoms, red spheres—constrained phosphorus atoms. (Color figure online)

To avoid boundary effects in *z*-direction once the pore is completely open (expanded pore stage) we developed a larger system hydrated with a greater number of water molecules.

In the small systems, we calculated the voltage generated by $E_0 + 50$ MV/m and $E_0 + 100$ MV/m at the initial configuration for the no constraint (NC) and the three constraint conditions (AC, CC, and ACC). The voltages were calculated as $V = E \times L_z$ where L_z is the size of the simulation box in the *z*-direction. In the large system we applied the electric field corresponding to the voltage calculated for the small system, taking into account the new size of the box in the *z*-direction for the NC, AC, CC, and ACC conditions (5 repetitions).

Pore Shape Modeling

In the simulations for each constraint condition the temporal evolution of pore shape and volume was monitored with a four-step algorithm. First the pore is centered inside the simulation box, a parallelepiped. The centering

procedure applies an offset to the *x, y*, and *z* coordinates in order to place the center of mass of the membrane at the center of the simulation box. In the second step the membrane is partitioned into three sections: the upper polar region, the internal non-polar region, and the lower polar region. Next the volume occupied by water molecules in the pore is sliced into cylindroids, cylinders with elliptical bases in the *x, y* plane, with a height of 0.1 nm in the *z*-direction (Fernández et al. 2012). Finally, as a simple metric for pore shape, angles for the cathodic (θ_C) and anodic (θ_A) sides (Fig. 2) are determined by the linear fit of the cylindroid radii from the center of the membrane to the ends of the pore (Fig. 2).

The measurements of the angles depicted in Figs. 2 and 3 correspond to a selected final geometry of the pore during the temporal evolution of the trajectory called an "expanded" pore, as explained in the next section.

Pore Opening Time

We define the pore opening time as the sum of the pore construction time and pore expansion time as described by Levine and Vernier (2012). The evolution of pore volume with time was modeled by fitting the simulation data to an exponential expression, Pore volume $(t) = \alpha + e^{t/\tau}$, where the parameters α and τ are the offset volume and the mean pore opening time, respectively, and t is the interval of the pore opening time. The mean pore opening time is the average time from pore initiation until the expanded pore condition is met.

Pore initiation time is the point at which all the cylindroids in the non-polar region of the membrane contain water molecules. This state corresponds to the so-called "hydrophobic pore" of some electroporation models. As the lipid head groups follow the water into the membrane interior, the pore increases in radius and volume. When the head groups from the two leaflets of the bilayer meet,

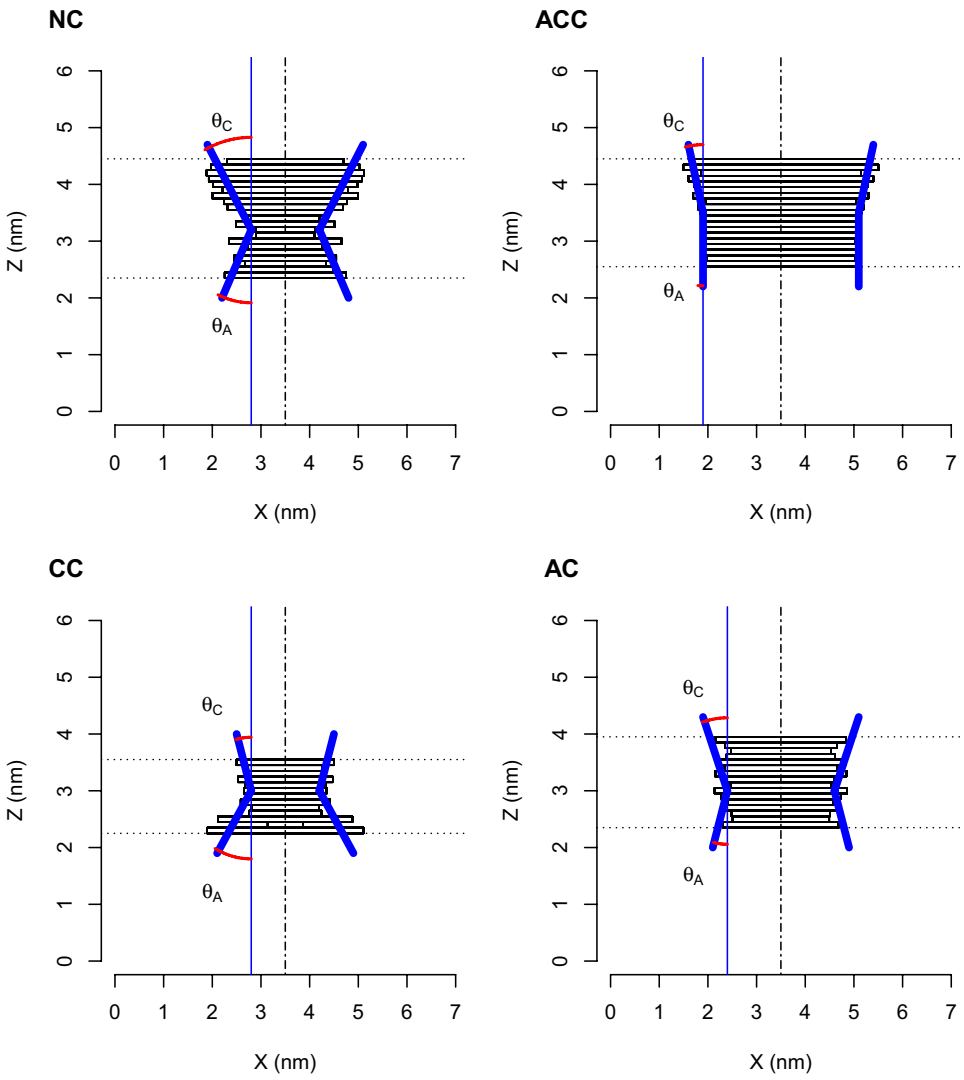

Fig. 2 Pore shape angles for anodic (θ_A) and cathodic (θ_C) leaflets, determined from a linear fit of the cylindroid radii (thick blue line). The thin vertical blue line is the radius of the cylindroid at the center of the membrane. The vertical dot-dashed line shows the center of the pore. The horizontal dotted lines are the borders of the internal, non-polar region of the bilayer. (Color figure online)

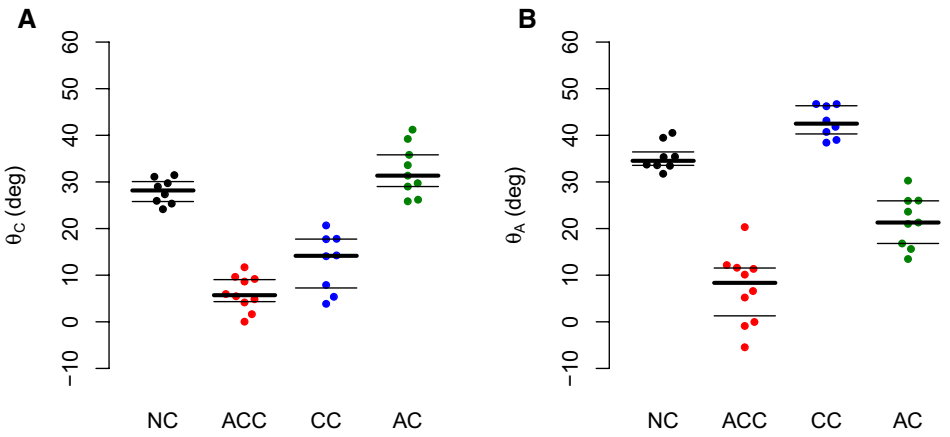

Fig. 3 Angles for **a** cathodic side (θ_C), and **b** anodic side (θ_A), for the four constraint conditions. Each dot is an individual simulation, black for NC, red for ACC, blue for CC, and green for AC. The thick line is the median, and the thin lines are the first and third quartiles. (Color figure online)

the configuration corresponds to the classical "hydrophilic pore."

For each condition, we selected a step in the pore-forming trajectory after the pore begins to expand but before the pore becomes too large relative to the simulated volume and the bilayer becomes disorganized. We called this structure an "expanded" pore. We ended the trajectory analysis with this expanded pore condition. Note that the magnitude of the porating electric field applied at this point is much larger than the range of stabilizing electric fields, so the system at this point is not in equilibrium. The time interval used for tracking the pore volume was from pore initiation until the expanded pore condition was reached. The boundaries for this interval are shown with dotted lines in Fig. 4.

We evaluate the evolution of the minimum radius, which is the radius of the smaller cylindroid that models the pore shape. The minimum radius is calculated as the mean of the radii in the x- and y-directions. For all constraint conditions, we call the pore "expanded" when the minimum radius reaches a value of 1 nm.

Data Processing

Molecular visualization was performed using Visual Molecular Dynamics, VMD (Humphrey et al. 1996). Analysis of the simulation trajectories was performed using custom programs developed in Python (Python). Statistical analysis was performed using the Wilcoxon non-parametric test. P values below 0.05 were considered significant. All statistical tests were performed in the R software environment (R Development Core Team 2016).

Results and Discussion

The minimum porating electric field E_0 serves as a metric for comparing bilayer systems with different properties (Ziegler and Vernier 2008). The E_0 found here for the no-constraint condition (350 MV/m) is consistent with previous reports for similar POPC systems (Gurtovenko and Lyulina 2014; Ziegler and Vernier 2008). E_0 increases under each of the constraint conditions: for the single constraint on the anodic side or the cathodic side, E_0 is 400 MV/m; for the double constraint on both anodic and cathodic sides, E_0 is 575 MV/m. Mechanical constraints on phospholipid head groups hinder, but do not prevent, pore formation in these systems. Previous MD reports showed that E_0 is increased in bilayers where the presence of cholesterol induces rigidity and restricts phospholipid movement (Fernández et al. 2010), and that adding a small amphiphilic molecule such as dimethyl sulfoxide capable of fluidizing the membrane reduces E_0 in lipid bilayers even in the presence of cholesterol (Fernandez and Reigada 2014). Reigada (2014) also showed that liquid-disordered regions of heterogeneous lipid bilayers are easier to electroporate than liquid-ordered regions. In simulations performed in single-component, POPC and palmitoyl-oleoyl-phosphatidylethanolamine (POPE) lipid bilayers, the POPE system shows a higher E_0 (600 MV/m) than the POPC system (400 MV/m). Authors explain the different responses of the two systems as a consequence of hydrogen bonds between POPE amine groups, which produce a more compact water–lipid interface than that found in POPC bilayers (Gurtovenko and Lyulina 2014).

We also found that mechanical constraints on the head group phosphorus atoms affect the shape of electropores (Fig. 1). For the no-constraint (NC) condition, the pore has the toroidal shape described previously (Tieleman 2004; Marrink et al. 2009). For anodic constraint (AC) and cathodic constraint (CC) conditions, the shape of the pore is axially asymmetrical. Although the lipids on the constrained side can move laterally in the plane of the bilayer to create an aqueous opening, they cannot move into the bilayer interior to participate in the formation of the pore walls, so the shape of the pore tends to be conical rather than toroidal. For the anode–cathode-constrained (ACC) condition, membrane-spanning water columns ("hydrophobic pores") are formed,

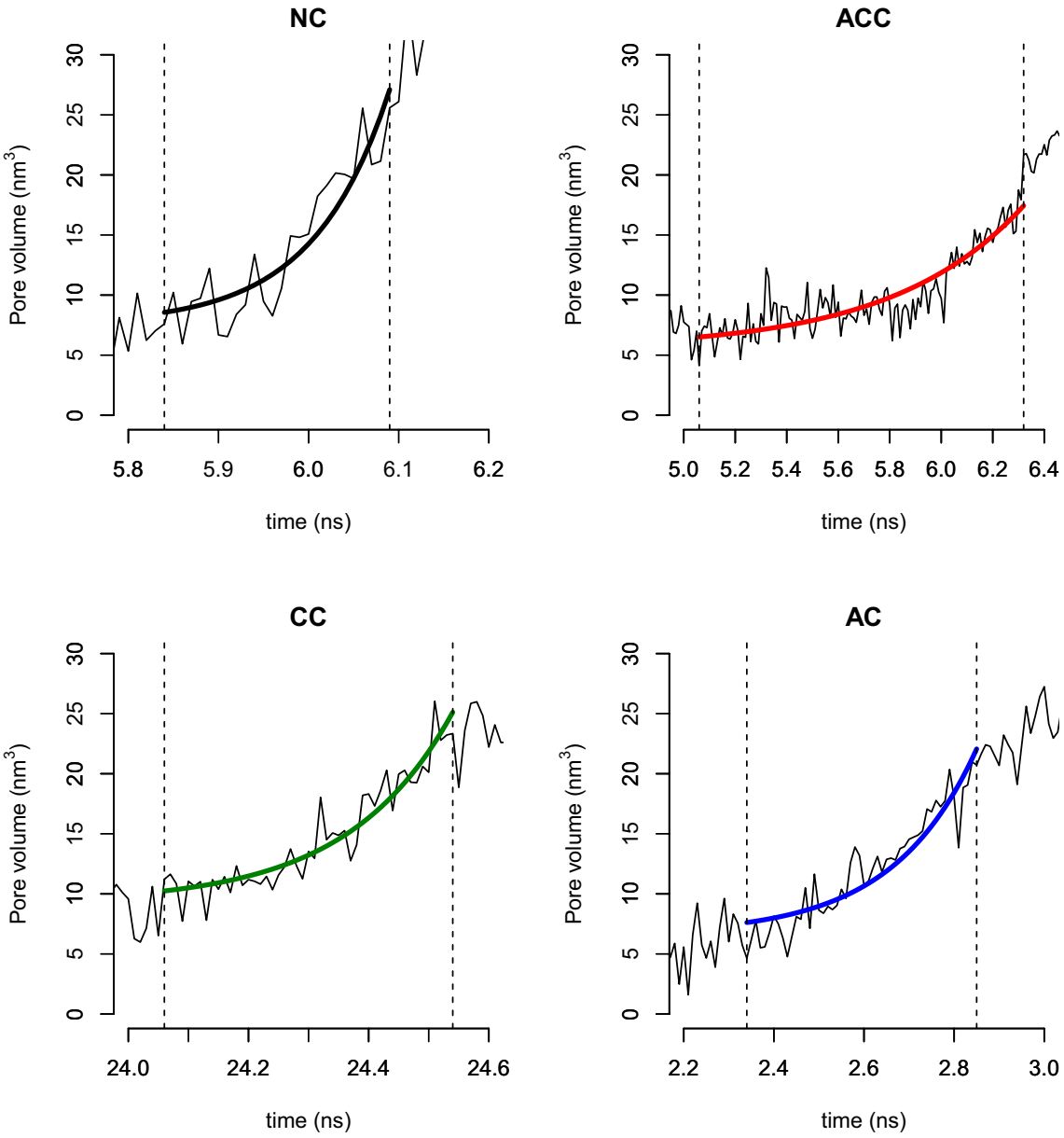

Fig. 4 Pore volume versus time (thin black lines) from representative simulations for each constraint condition, where the thicker lines show the exponential fit between the time of pore initiation and the end of pore expansion as defined in the "Methods" (dotted lines), black for NC, red for ACC, blue for CC, and green for AC. (Color figure online)

since no lipid head group is allowed to move out of the plane of the bilayer.

To characterize and model the shape of the pores obtained in the different conditions we extracted cathodic (θ_C) and anodic (θ_A) pore angles from the geometry of the "expanded pore," as shown in Fig. 2. Figure 3 shows that the median pore angles are relatively large for both leaflets for the NC condition ($\theta_C = 28°$, $\theta_A = 35°$; $P < 0.001$), reflecting the toroidal shape of these pores. The angle for the ACC condition is narrow for both leaflets ($\theta_C = 6°$, $\theta_A = 8°$; $P =$ NS), following the roughly cylindrical shape of the membrane-spanning water column. Angles for the CC and AC conditions reflect the conical shape of these pores. The CC pore angles are wider on the anode side ($\theta_C = 14°$, $\theta_A = 42°$; $P < 0.001$), and the AC pores are wider on the cathode side ($\theta_C = 31°$, $\theta_A = 21°$; $P < 0.05$).

The differences among the angles for the four conditions in the cathodic leaflet are statistically significant for NC versus ACC and CC ($P < 0.001$), and for AC versus ACC and CC ($P < 0.001$) while the differences among NC versus AC and ACC versus CC are NS. The differences among the angles for the four conditions in the anodic leaflet

are statistically significant for NC versus ACC and AC ($P < 0.001$), for ACC versus CC and AC ($P < 0.001$), and for CC versus AC ($P < 0.001$), while the differences among NC versus CC are NS.

For the cathodic and anodic constraint conditions, the pore that is formed is lined with head groups, and so can be called "hydrophilic," but the shape is conical rather than toroidal (no constraints) or cylindrical (constraints on both leaflets). The lipid head groups that form the walls of these conical pores come only from the unconstrained leaflet. This type of electropore also appears transiently in simulations of POPC:POPE asymmetric bilayers, where only the POPC head groups are involved in pore initiation, and only later in the process do the POPE head groups migrate into the membrane interior, with the result being finally a toroidal symmetrical pore (Gurtovenko and Lyulina 2014).

Pore formation occurs even with the head groups constrained on both sides of the bilayer, but these pores are water bridges with a roughly cylindrical profile, not so-called hydrophilic pores, since the head groups cannot follow the water into the membrane interior. Similar structures have been described in water/octane systems (Tieleman 2004) in water–vacuum–water systems (Ho et al. 2013), for anionic lipid bilayers composed only of palmitoyl-oleoyl-phosphatidylserine (POPS) (Dehez et al. 2014), and for archaeal lipid bilayers (Polak et al. 2014).

If the conical pore shape corresponds to structures formed in cell membranes, it may be at least in part responsible for the ion current rectification reported in the observations of cells exposed to an external electric field or in artificial pores formed in polymeric foils (Pakhomov et al. 2009; Siwi et al. 2002).

Figure 4 shows the evolution of the pore volume with time from representative simulations for each constraint condition. Figure 5 shows the median and interquartile pore volume versus time. The medians of the mean pore opening time (τ) are: 0.10 ns for NC, 0.42 ns for ACC, 0.16 ns for CC, and 0.22 ns for AC. The differences among the pore opening times for the various conditions are statistically significant. These results show that the constraints affect pore opening dynamics (Fig. 5). Constraints on one side of the bilayer (anodic or cathodic) slow pore opening. This effect seems to be more pronounced in the AC system. Constraints on both sides have an even greater retarding effect.

Pakhomov et al. have reported evidence for asymmetric (rectifying) lipid pores, which could be associated with interactions of the membrane with the cytoskeleton or the extracellular matrix (Pakhomov and Pakhomova 2010). Consistent with this idea, modifications of cytoskeletal organization have been correlated with exposures to porating electric fields in several different systems (Rols and Teissié 1992; Teissié and Rols 1994; Kanthou et al. 2006; Berghöfer et al. 2009; Rosazza et al. 2011 Chopinet et al. 2014; Thompson et al. 2014). These permeabilization-induced perturbations of membrane–cytoskeleton associations may restrict in various ways the movements of membrane lipids, resulting in asymmetric, non-toroidal pores.

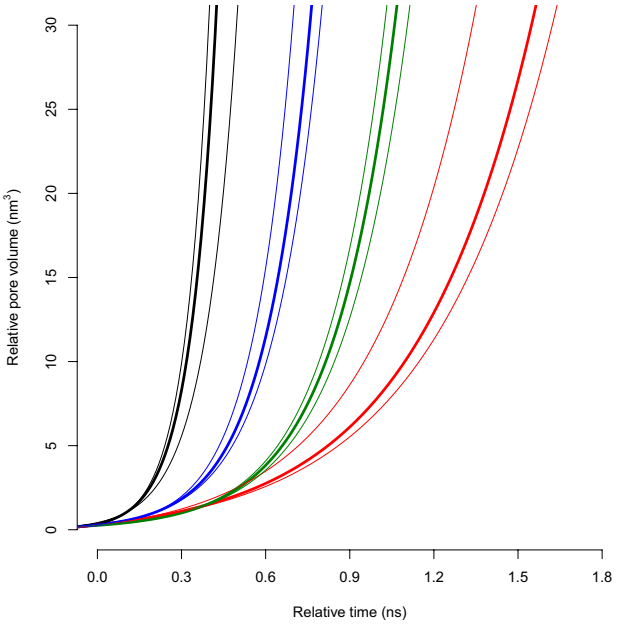

Fig. 5 Relative pore volume versus time for each constraint condition, where black is NC, red is ACC, blue is CC, and green is AC. The relative pore volume was obtained by imposing an offset volume from the exponential model of the pore opening, with $\alpha = 1$, to all conditions and the relative time was obtained by subtracting the initiation time from all simulations. The heavy solid lines are the median value of all simulations for each condition; the lighter lines are first and third quartile. (Color figure online)

In summary, our results show that molecular models of lipid membrane electropores with several shapes and symmetries can be obtained by mechanically constraining the lipids that compose the bilayer. The variations in pore properties arising from this geometrical heterogeneity may help to explain, at least in part, the origin of the broad distribution of size and lifetime in populations of permeabilizing structures in electroporated cells.

Acknowledgements Computational resources were provided by the Centro de Cómputos de Alto Rendimiento (CeCAR) - Facultad de Ciencias Exactas y Naturales – UBA and ITBA. PTV was supported by the Frank Reidy Research Center for Bioelectrics and by the Air Force Office of Scientific Research (FA9550-14-1-0123 and MURI grant FA9550-15-1-0517 on "Nanoelectropulse-Induced Electromechanical Signaling and Control of Biological Systems," administered through Old Dominion University). MLF and MR were supported in part by grants from Universidad de Buenos Aires (UBACyT GC 20620130100027BA), CONICET (PIP GI 11220110100379) and ITBA (ITBACyT 2015), and MR received additional support from IBM of Argentina. MLF and MR gratefully acknowledge the guidance of Professor G. Marshall.

References

Berendsen HJC, Postma JPM, van Gunsteren WF, Hermans J (1981) Interaction models for water in relation to protein hydration. In: Pullman B (ed) Intermolecular forces. Reidel, Dordrecht, pp 341–342

Berendsen HJC, Postma JPM, van Gunsteren WF, DiNola A, Haak JR (1984) Molecular dynamics with coupling to an external bath. J Chem Phys 81:3684–3690

Berger O, Edholm O, Jahnig F (1997) Molecular dynamics simulations of a fluid bilayer of dipalmitoylphosphatidylcholine at full hydration, constant pressure, and constant temperature. Biophys J 72:2002–2013

Berghöfer T, Eing C, Flickinger B, Hohenberger P, Wegner LH, Frey W, Nick P (2009) Nanosecond electric pulses trigger actin responses in plant cells. Biochem Biophys Res Commun 387:590–595

Breton M, Mir LM (2012) Microsecond and nanosecond electric pulses in cancer treatments. Bioelectromagnetics 33:106–123

Chopinet L, Etienne D, Rols MP (2014) AFM sensing cortical actin cytoskeleton destabilization during plasma membrane electropermeabilization. Cytoskeleton 71:587–594

DeBruin KA, Krassowka W (1999) Modeling electroporation in a single cell. I. Effects of field strength and rest potential. Biophys J 77:1213–1224

Dehez F, Delemotte L, Kramar P, Miklavčič D, Tarek M (2014) Evidence of conducting hydrophobic nanopores across membranes in response to an electric field. J Phys Chem C 118:6752–6757

Essman U, Perera L, Berkowitz ML, Darden HTL, Pedersen LG (1995) A smooth particle mesh Ewald method. J Chem Phys 103:8577–8593

Fernández ML, Marshall G, Sagués F, Reigada R (2010) Structural and kinetic molecular dynamics study of electroporation in cholesterol-containing bilayers. J Phys Chem B 114:6855–6865

Fernández ML, Reigada R (2014) Effects of dimethyl sulfoxide on lipid membrane electroporation. J Phys Chem B 118:9306–9312

Fernández ML, Risk MR, Reigada R, Vernier PT (2012) Size-controlled nanopores in lipid membranes with stabilizing electric fields. Biochem Biophys Res Commun 423:325–330

Gurtovenko AA, Lyulina AS (2014) Electroporation of asymmetric phospholipid bilayers. J Phys Chem B 118:9909–9918

Hess B, Bekker H, Berendsen HJC, Fraaije JGEM (1997) LINCS: a linear constraint solver for molecular simulations. J Comput Chem 18:1463–1472

Hess B, Kutzner C, van der Spoel D, Lindahl E (2008) GROMACS 4: algorithms for highly efficient, load-balanced, and scalable molecular simulation. J Chem Theory Comput 4:435–447

Ho MC, Levine ZA, Vernier PT (2013) Nanoscale, electric field-driven water bridges in vacuum gaps and lipid bilayers. J Membr Biol 246:793–801

Humphrey W, Dalke A, Schulten K (1996) VMD—visual molecular dynamics. J Mol Graph 14:33–38. http://www.ks.uiuc.edu/Research/vmd/

Ingólfsson HI, Melo MN, van Eerden FJ, Arnarez C, Lopez CA, Wassenaar TA, Periole X, de Vries AH, Tieleman DP, Marrink SJ (2014) Lipid organization of the plasma membrane. J Am Chem Soc 136:14554–14559

Joshi RP, Hu Q (2010) Analysis of the cell membrane permeabilization mechanics and pore shape due to ultrashort electrical pulsing. Med Biol Eng Comput 48:837–844

Kanthou C, Kranjc S, Sersa G, Tozer G, Zupanic A, Cemazar M (2006) The endothelial cytoskeleton as a target of electroporation-based therapies. Mol Cancer Ther 5:3145–3152

Kiessling V, Crane JM, Tamm LK (2006) Transbilayer effect of raft-like domains in asymmetric planar bilayers measured by single molecule tracking. Biophys J 91:3313–3326

Kotnik T, Frey W, Sack M, Meglič SH, Peterka M, Miklavčič D (2015) Electroporation-based applications in biotechnology. Trends Biotechnol 33:480–488

Kotulska M, Dyrka W, Sadowsi P (2010) Fluorescent methods in evaluation of nanopore conductivity and their computational validation. In: Pakhomov AG, Miklavčič D, Markov MS (eds) Advanced electroporation techniques in biology and medicine. CRC Press, Taylor & Francis Group, Boca Raton, pp 123–139

Levine ZA, Vernier PT (2010) Life cycle of an electropore: field-dependent and field-independent steps in pore creation and annihilation. J Membr Biol 236:27–36

Levine ZA, Vernier PT (2012) Calcium and phosphatidylserine inhibit lipid electropore formation and reduce pore lifetime. J Membr Biol 245:599–610

Lyubartsev AP, Rabinovich AL (2016) Force field development for lipid membrane simulations. Biochim Biophys Acta 1828:2483–2497

MacCallum JL, Bennett WFD, Tieleman DP (2008) Distribution of amino acids in a lipid bilayer from computer simulations. Biophys J 94:3393–3404

Marrink SJ, de Vries AH, Tieleman DP (2009) Lipids on the move: Simulations of membrane pores, domains, stalks and curves. Biochim Biophys Acta 1788:149–168

Mihajlovic M, Lazaridies T (2010) Antimicrobial peptides in toroidal and cylindrical pores. Biochim Biophys Acta 1798:1485–1493

Miyamoto S, Kollman PA (1992) SETTLE: an analytical version of the SHAKE and RATTLE algorithms for rigid water models. J Comput Chem 13:952–962

Ollila OH, Pabst G (2016) Atomistic resolution structure and dynamics of lipid bilayers in simulations and experiments. Biochim Biophys Acta 1858:2512–2528

Pakhomov AG, Bowman AM, Ibey BL, Andre FM, Pakhomova ON, Schoenbach KH (2009) Lipid nanopores can form stable, ion channel-like conduction pathway in cell membrane. Biochem Biophys Res Commun 385:181–186

Pakhomov AG, Pakhomova ON (2010) Nanopores: a distinct transmembrane passageway in electroporated cells. In: Pakhomov AG, Miklavčič D, Markov MS (eds) Advanced electroporation techniques in biology and medicine. CRC Press, Taylor & Francis Group, Boca Raton, pp 177–194

Polak A, Bonhenry D, Dehez F, Kramar P, Miklavčič D, Tarek M (2013) On the electroporation thresholds of lipid bilayers: molecular dynamics simulation investigations. J Membr Biol 246:843–850

Polak A, Tarek M, Tomšič M, Valant J, Poklar Ulrihe N, Jamnik A, Kramar P, Miklavčič D (2014) Electroporation of archaeal lipid membranes using MD simulations. Bioelectrochemistry 100:18–26

Python http://www.python.org

R Development Core Team (2016) R: a language and environment for statistical computing. R Foundation for Statistical Computing, Vienna

Raghupathy R, Anilkumar AA, Polley A, Singh PP, Yadav M, Johnson C, Suryawanshi S, Saikam V, Sawant SD, Panda A, Guo Z, Vishwakarma RA, Rao M, Mayor S (2015) Transbilayer lipid interactions mediate nanoclustering of lipid-anchored proteins. Cell 161:581–594

Reigada R (2014) Electroporation of heterogeneous lipid membranes. Biochim Biophys Acta 1838:814–821

Risselada HJ, Mark AE, Marrink SJ (2008) Application of mean field boundary potentials in simulations of lipid vesicles. J Phys Chem B 112:7438–7447

Rols MP, Teissié J (1992) Experimental evidence for the involvement of the cytoskeleton in mammalian cell electropermeabilization. Biochim Biophys Acta 1111:45–50

Rosazza C, Escoffre JM, Zumbusch A, Rols MP (2011) The actin cytoskeleton has an active role in the electrotransfer of plasmid DNA in mammalian cells. Mol Ther 19:913–921

Sapay N, Bennett WFD, Tieleman DP (2009) Thermodynamics of flip-flop and desorption for a systematic series of phosphatidylcholine lipids. Soft Matter 5:3295–3302

Sengupta D, Leontiadou H, Mark AE, Marrink SJ (2008) Toroidal pores formed by antimicrobial peptides show significant disorder. Biochim Biophys Acta Biomembr 1778:2308–2317

Silve A, Brunet AG, Al-Sakere B, Ivorra A, Mir LM (2014) Comparison of the effects of the repetition rate between microsecond and nanosecond pulses: electropermeabilization-induced electrodesensitization? Bichem Biophys Acta 1840:2139–2151

Siwi Z, Gu Y, Spohr HA, Baur D, Wolf-Reber A, Spohr R, Apel P, Korchev YE (2002) Rectification and voltage gating of ion currents in a nanofabricated pore. Europhys Lett 60:349–355

Smith KC, Weaver JC (2011) Transmembrane molecular transport during versus after extremely large, nanosecond electric pulses. Biochem Biophys Res Commun 412:8–12

Son RS, Smith KC, Gowrishankar TR, Vernier PT, Weaver JC (2014) Basic features of a cell electroporation model: Illustrative behavior for two very different pulses. J Membr Biol 247:1209–1228

Stacey M, Fox P, Buescher S, Kolb J (2011) Nanosecond pulsed electric field induced cytoskeleton, nuclear membrane and telomere damage adversely impact cell survival. Bioelectrochemistry 82:131–134

Stoddart D, Ayub M, Höfler L, Raychaudhuri P, Klingelhoefer JW, Maglia G, Heron A, Bayley H (2014) Functional truncated membrane pores. Proc Natl Acad Sci USA 111:2425–2430

Sugar IP, Neumann E (1984) Stochastic model for electric field-induced membrane pores electroporation. Biophys Chem 19:211–225

Sun S, Yin G, Lee YK, Wong JT, Zhang TY (2011) Effects of deformability and thermal motion of lipid membrane on electroporation: by molecular dynamics simulations. Biochem Biophys Res Commun 404:684–688

Tarek M (2005) Membrane electroporation: a molecular dynamics study. Biophys J 88:4045–4053

Teissié J, Rols MP (1994) Manipulation of cell cytoskeleton affects the lifetime of cell membrane electropermeabilization. Ann N Y Acad Sci 720:98–110

Tieleman DP (2004) The molecular basis of electroporation. BMC Biochem 5:10

Thompson GL, Roth C, Tolstykh G, Kuipers M, Ibey BL (2014) Disruption of the actin cortex contributes to susceptibility of mammalian cells to nanosecond pulsed electric fields. Bioelectromagnetics 35:262–272

Tsong T (1991) Electroporation of cell membranes. Biophys J 60:297–306

Weaver JC, Chizmadzhev YA (1996) Theory of electroporation: a review. Bioelectrochem Bioenerg 41:135–160

Weaver JC (2000) Electroporation of cells and tissues. IEEE Trans Plasma Sci 28:24–33

Yarmush ML, Golberg A, Serša G, Kotnik T, Miklavčič D (2014) Electroporation-based technologies for medicine: principles, applications, and challenges. Annu Rev Biomed Eng 16:295–320

Ziegler MJ, Vernier PT (2008) Interface water dynamics and porating electric field for phospholipid bilayers. J Phys Chem B 112:13588–13596